

Article

Geological Constraints on the Gas-Bearing Properties in High-Rank Coal: A Case Study of the Upper Permian Longtan Formation from the Songzao Coalfield, Chongqing, Southwest China

Dishu Chen ^{1,2,3} , Jinxi Wang ^{1,2}, Xuesong Tian ^{1,2,*} , Dongxin Guo ^{1,2}, Yuelei Zhang ^{1,2} and Chunlin Zeng ^{1,2}

¹ Key Laboratory of Shale Gas Exploration, Ministry of Natural Resources, Chongqing Institute of Geology and Mineral Resources, Chongqing 401120, China; cds1003chengdu@163.com (D.C.); m17347807272@163.com (J.W.); shmilydongxin@163.com (D.G.); zyl7049@163.com (Y.Z.); ceng8623@189.cn (C.Z.)

² National and Local Joint Engineering Research Center of Shale Gas Exploration and Development, Chongqing Institute of Geology and Mineral Resources, Chongqing 401120, China

³ School of Earth Resources, China University of Geosciences (Wuhan), Wuhan 430074, China

* Correspondence: xuesongtian@outlook.com; Tel.: +86-15205155670

Abstract: The Permian Longtan Formation in the Songzao coalfield, Southwest China, has abundant coalbed methane (CBM) stored in high-rank coals. However, few studies have been performed on the mechanism underlying the differences in CBM gas content in high-rank coal. This study focuses on the characterization of coal geochemical, reservoir physical, and gas-bearing properties in the coal seams M₆, M₇, M₈, and M₁₂ based on the CBM wells and coal exploration boreholes, discusses the effects of depositional environment, tectono-thermal evolution, and regional geological structure associated with CBM, and identifies major geological constraints on the gas-bearing properties in high-rank coal. The results show that high-rank coals are characterized by high TOC contents (31.49~51.32 wt%), high T_{max} and R₀ values (averaging 539 °C and 2.17%), low HI values (averaging 15.21 mg of HC/g TOC), high porosity and low permeability, and high gas-bearing contents, indicating a post-thermal maturity and a good CBM production potential. Changes in the shallow bay–tidal flat–lagoon environment triggered coal formation and provided the material basis for CBM generation. Multistage tectono-thermal evolution caused by the Emeishan mantle plume activity guaranteed the temperature and time for overmaturation and thermal metamorphism and added massive pyrolytic CBM, which improved the gas production potential. Good geological structural conditions, like enclosed fold regions, were shown to directly control CBM accumulation.

Keywords: coalbed methane enrichment; Permian Longtan Formation; high-rank coal; depositional environment; tectono-thermal evolution; regional geological structure



Citation: Chen, D.; Wang, J.; Tian, X.; Guo, D.; Zhang, Y.; Zeng, C. Geological Constraints on the Gas-Bearing Properties in High-Rank Coal: A Case Study of the Upper Permian Longtan Formation from the Songzao Coalfield, Chongqing, Southwest China. *Energies* **2024**, *17*, 1262. <https://doi.org/10.3390/en17051262>

Academic Editor: Changkook Ryu

Received: 30 January 2024

Revised: 29 February 2024

Accepted: 4 March 2024

Published: 6 March 2024



Copyright: © 2024 by the authors. Licensee MDPI, Basel, Switzerland. This article is an open access article distributed under the terms and conditions of the Creative Commons Attribution (CC BY) license (<https://creativecommons.org/licenses/by/4.0/>).

1. Introduction

Abundant coalbed methane (CBM) resources are stored in high-rank coals in China, representing a geological resource of $1.044 \times 10^{13} \text{ m}^3$, which accounts for approximately one-third of the total CBM resources [1–3]. Realizing the development and utilization of high-rank CBM plays an important and reliable role in guaranteeing national green energy security, reducing the hazards of coal mine gas, and decreasing carbon dioxide emissions [4–7]. To date, high-rank CBM has garnered extensive attention, with major breakthroughs and commercial developments in the Jincheng and Shouyang–Yangquan areas (Qingshui basin) in North China, the southern part of the Hancheng–Yanchuan area (Ordos basin), and several areas of the Qianbei–Qianxi–Chuannan area in Southwest China [8–13].

However, to efficiently increase the supply of green energy and successfully achieve the carbon peak and carbon neutrality in China by 2030 and 2060, high-rank CBM exploration

and development should be carried out immediately. Some areas that have not been extensively explored for high-rank CBM in Southwest China will become a major focus of research, such as typical coalfields distributed in Chongqing city. Chongqing city is rich in high-rank CBM resources, with a conservative value of $2 \times 10^{11} \text{ m}^3$. In particular, the CBM resources from the Songzao coalfield account for 65.7% of the total resources, with $2 \times 10^8 \text{ m}^3/\text{km}^2$, indicating a great resource potential. In addition, the Songzao coalfield is also an important anthracite production base [14] and one of the coalfields with the most serious coal and gas outburst accidents in China. Therefore, the Songzao coalfield is an ideal area for further exploration, development, and utilization of high-rank CBM resources in Chongqing city, Southwest China.

Previous studies effectively summarized the systematic geologic theory of high-rank CBM formation in the carboniferous Taiyuan Formation and Permian Shanxi Formation of the Jincheng area and Shouyang–Yangquan areas within the Qinshui basin, including their geochemistry, reservoir physical, and gas-bearing properties, accumulation mechanism, enrichment pattern, main controlling factors, a geological model, and a resource prospect [9,12,15–22]. High-rank CBM reservoirs are highly diverse, complex, and heterogeneous, with limited permeability, undersaturation, low pressure, overmaturation, and high gas contents. However, there are distinct geological variables impacting high-rank CBM accumulation in different regions of China, posing hurdles to improving the CBM production potential [2,15,23,24]. Compared with the great progress regarding high-rank CBM within the Qinshui basin in North China, although some geological investigations on high-rank CBM in the Permian Longtan Formation in the northern and western parts of Guizhou province in Southwest China were conducted [8,10,25–29], the geological characteristics of high-rank CBM in the Songzao coalfield in Chongqing are still lacking in pertinence and validity, and CBM exploration has not yet achieved a major breakthrough. A detailed study of the geological constraints on the CBM gas content in the high-rank coals of the Longtan Formation from the coalfield is thus indispensable.

In this study, coal geochemical, coal reservoir physical, and gas-bearing properties of the main high-rank coal seams in the Longtan Formation in the Songzao coalfield of Chongqing city were analyzed. The effects of depositional environment, tectono-thermal evolution, and regional geological structural conditions on coal formation, CBM gas production potential, and gas accumulation in high-rank coals are comprehensively discussed, and major geological constraints on the gas-bearing properties of high-rank coal from the Longtan Formation in the Songzao Coalfield are identified.

2. Geological Setting

The Songzao coalfield is situated in the Qijiang District in the southwestern part of Chongqing city in Southwest China and has a total area of approximately 235.5 km^2 (Figure 1a,b). It mainly consists of twelve key coal mines, i.e., the Songzao, Tonghua, Guanyinqiao, Yangchatan, Yuyang, Datong, Shihao, Zhangshiba, Liyuanba, Daluo, Xiaoyutuo, and Macun mines (Figure 1b).

2.1. Regional Structural Features

The coalfield is located in the secondary fold belt on the western flank of the Jiudianya, Jiulongshan, and Sangmuchang anticlines (Figure 1b). Its structural pattern presents a radial shape that converges to the northeast and spreads to the southwest. The Lianghekou syncline, Yangchatan anticline, Damushu syncline, and Yutiao anticline from east to west in the coalfield form a “bulge-shaped structure” to the northwestward rise. This structure is distinguished by wide, low anticlines and compact synclines with a gradual weakening of fold amplitude from east to west. Surface fracture phenomena are relatively insignificant and minor, and only those associated with the four folds affect the mining conditions. In addition, the stratigraphic denudation in the anticline cores is more serious than that in the syncline cores, the extension direction of the fracture zones is nearly parallel or perpendicular to the anticline axis, and the fracture extensions are not far.

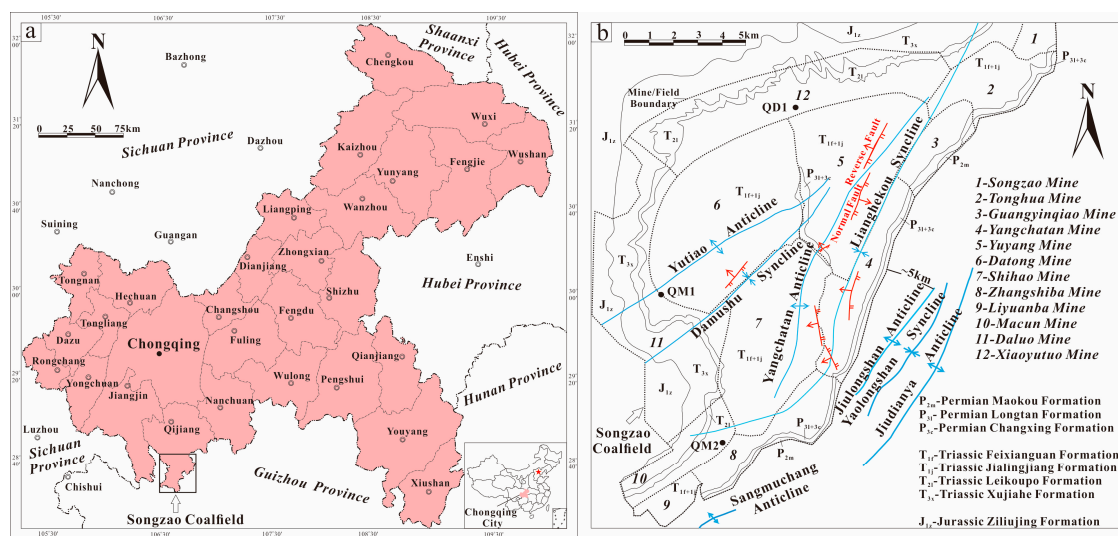


Figure 1. (a) Location of the Songzao coalfield in Chongqing city, Southwest China; (b) regional structural and lithostratigraphic divisions of the Songzao coalfield.

2.2. Regional Structural Features

The coalfield is located in the secondary fold belt on the western flank of the Jiudianya, Jiulongshan, and Sangmuchang anticlines (Figure 1b). Its structural pattern presents a radial shape that converges to the northeast and spreads to the southwest. The Lianghekou syncline, Yangchatan anticline, Damushu syncline, and Yutiao anticline from east to west in the coalfield form a “bulge-shaped structure” to the northwestward rise. This structure is distinguished by wide, low anticlines and compact synclines with a gradual weakening of fold amplitude from east to west. Surface fracture phenomena are relatively insignificant and minor, and only those associated with the four folds affect the mining conditions. In addition, the stratigraphic denudation in the anticline cores is more serious than that in the syncline cores, the extension direction of the fracture zones is nearly parallel or perpendicular to the anticline axis, and the fracture extensions are not far.

2.3. Coal-Bearing Stratigraphic Characteristics

The strata exposed in the coalfield mainly include the Paleozoic Permian series and the Mesozoic Triassic and Jurassic series (Figure 1b). The Jurassic and Triassic strata are widely distributed in the synclines in the western, eastern, and southeastern parts of the coalfield, while the Permian strata are mainly exposed along the anticline axis or near the axis in the eastern and southeastern parts of the coalfield. By the latest Permian integrative stratigraphy and timescale of China [30], the upper Permian series in the coalfield include the Wuchiapingian and Changhsingian stages. The Changhsingian stage includes the Changxing Formation, and the Wuchiapingian stage includes the Longtan Formation.

The coal measure strata of the coalfield are exposed in the Longtan Formation, which mainly consists of coal seams, bioclastic and siliceous limestone, sandstone, siltstone, silty mudstone, calcareous mudstone, argillaceous shale, and tuffaceous sediments, and belong to the shallow bay–tidal flat–lagoon mixed deposits of alternating marine–continental transitional environments along the western margin of a shallow carbonate platform within an epicontinental sea ([14,31–37] and Figure 1). The Kangdian Oldland is the dominant terrestrial source for the coalfield. The total thickness of the coal measure strata is generally approximately 66 to 80 m, containing 5 to 13 coal seams with a high metamorphic degree (type III kerogen) and an average maximum vitrinite reflectance (R_0 , max) greater than 2.0%, among which, the main coal seams include M₆, M₇, M₈, and M₁₂ throughout the whole coalfield, which are important targets of CBM exploration and development (Figure 2). The middle Permian Maokou Formation disconformably underlies the Longtan coal measure strata, which consists of medium-to-thick-bedded and massive bioclastic

limestones that are rich in marine fossils, mostly including fusulinids, corals, brachiopods, ammonites, conodonts, benthic foraminifera, and calcareous algae [38,39]. The Longtan Formation overlies the Changxing Formation, which is composed of medium-to thick-bedded bioclastic limestone containing less dolomite and less banded and nodular cherts dominated by marine fusulinid, coral, brachiopod, and ammonite fossils in a shallow carbonate platform environment.

Series	Stage	Formation	Member	Histogram	Lithologic Character	Thickness (m)	Stability and Recoverability of Main Coal Seams
Upper Permian Series	Changhsingian Stage	Changxing Formation			Bioclastic limestone containing less dolomite and less banded and nodular cherts with the dominated marine fossils fusulinids, coral, brachiopods and ammonites		
	Wuchiapingian Stage	Longtan Formation	Fifth Member		Calcareous mudstone, siltstone intercalated with limestone	3~10	
			Fourth Member		Bioclastic limestone, siliceous limestone intercalated with mudstone and siltstone <i>Xianyuan Limestone</i>	5~30	
			Third Member		<i>Zhangshiba Limestone</i> Coal seam M_6 Coal seam M_7 Calcareous mudstone, silty mudstone, siltstone intercalated with fine sandstone, tonstein and limestone layers <i>LiYuanba Limestone</i> Coal seam M_{9-99}	20~60	M_6 and M_7 : Relatively stable Locally recoverable M_8 : Stable Recoverable M_9 : Unstable Locally recoverable
			Second Member		Bioclastic limestone, siliceous limestone intercalated with mudstone <i>Liangcun-Wenshui Limestone</i>	2~37	
First Member		Coal seam M_{10-11} Mudstone, siltstone, fine sandstone intercalated with the limestone and tonstein layers <i>Guanyinqiao Limestone</i> Coal seam M_{12} Bauxitic mudstone and kaolinite tonstein	10~45	M_{10} and M_{11} : Unstable Locally recoverable M_{12} : Relatively stable Locally recoverable			
Middle Permian Series	Roadian, Wordian, Capitanian Stages	Maokou Formation			Bioclastic limestone with rich fossils, such as fusulinids, corals, brachiopods, ammonites, conodonts, foraminifera and calcareous algae		

Figure 2. Typical lithologic stratigraphic framework of the Permian Longtan Formation in the Songzao coalfield.

2.4. Thickness and Distribution of the Main Coal Seams

The thickness and distribution of the main coal seams M_6 , M_7 , M_8 , and M_{12} in the Longtan Formation in the Songzao coalfield are relatively stable (Figures 2 and 3 and Table 1). The coal seams are usually buried at a depth of 400~1700 m, and their total thickness is 4.01~9.88 m, with an average of 7.58 m and a total recoverable value of 5.45 m. There is a thinning zone with a range of 2 km² in the northwestern part of the coalfield, which is situated at the junction of the Xiaoyutuo and Daluo mines. The total thickness of the four coal seams averages approximately 3 m, but their largest area, distributed in the Shihao, Datong, and Daluo mines located on the southeastern flank of the Damushu syncline, has a total thickness of approximately 8 m. But in the monoclinical structure in the southwestern area of the coalfield, the thickness of the four coal seams is generally small.

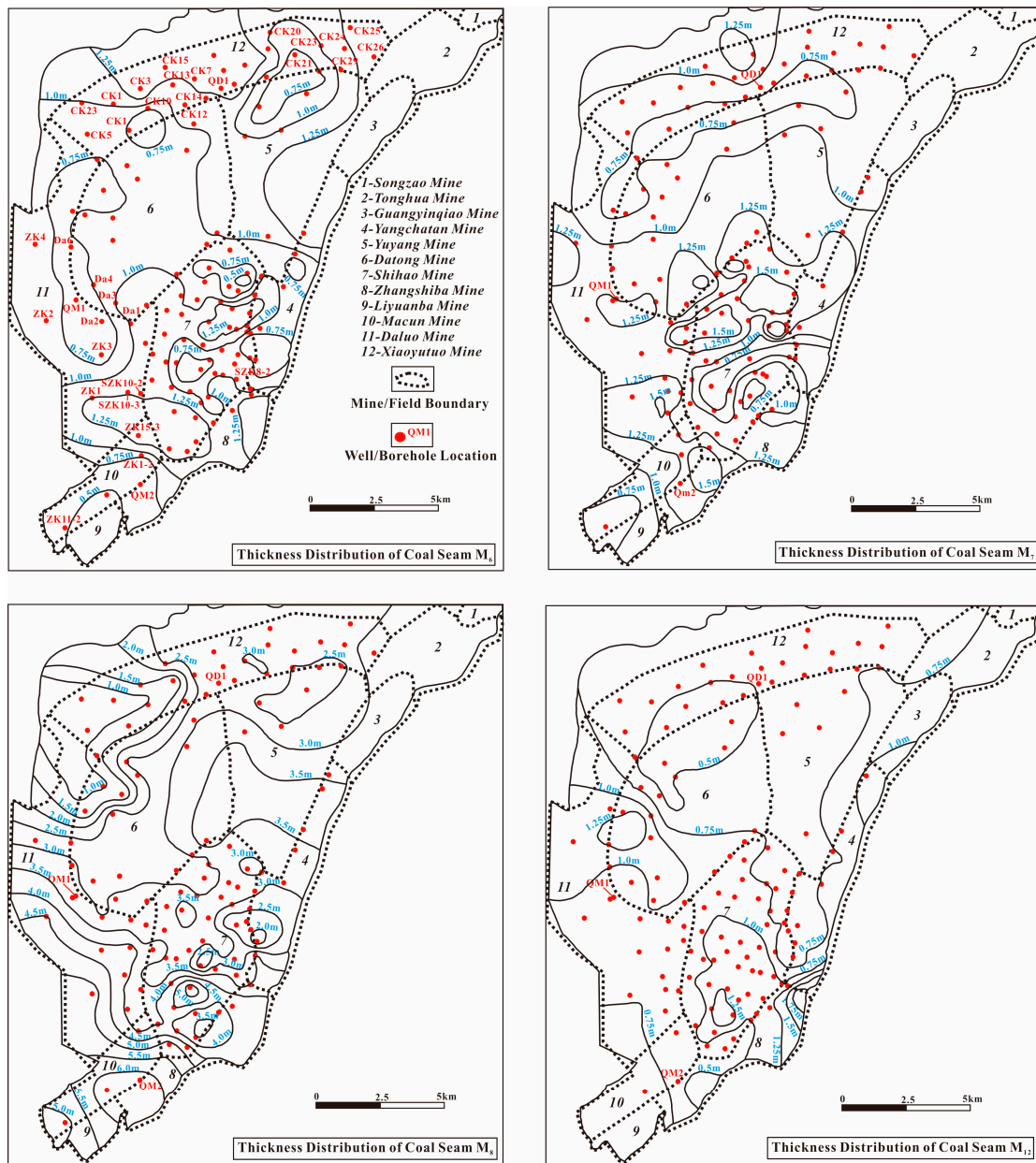


Figure 3. Thickness variation in the coal seams M₆, M₇, M₈, and M₁₂.

Table 1. General parameters of the coal seams M₆, M₇, M₈, and M₁₂.

Coal Seam Number	Depth of Coal Seams (m)	Thickness (m) Minimum–Maximum Average	Coal Seam Interlayer Spacings (m)	Tonstein Thickness (m) Minimum–Maximum Average	Lithological Characters of Coal Seam Roof and Floor		Stable and Recoverable
					Coal Seam Floor	Coal Seam Roof	
M ₆	400–1700	0.4–1.47 0.94	7.1	0.03–0.24 0.11	mudstone–siltstone	mudstone–siltstone	relatively stable locally recoverable
M ₇		0.71–1.62 1.11		0.01–0.57 0.26	mudstone–siltstone	mudstone	relatively stable locally recoverable
M ₈		0.83–6.43 3.04	6.6	0.03–0.58 0.24	sandstone–siltstone	mudstone–siltstone	stable recoverable
M ₁₂		0.31–3.33 0.86		0.01–0.1 0.04	siltstone–sandy mudstone	siltstone–sandy mudstone	relatively stable locally recoverable

The coal seams M₆, M₇, and M₈ are located in the middle part of the Longtan coal measure strata, with interlayer spacings of 7.1 m and 6.6 m. The thickness of the coal seams

M₇ and M₈ revealed a trend of gradual increase as the depth increased. The coal seam M₁₂ is located in the lower part of the coal measure strata, with an interlayer separation of approximately 22.6 m from the coal seam M₈. The total thickness of the coal seam M₆ is 0.4~1.47 m, with an average of 0.94 m, and it serves as an unstable coal seam, containing 0~1 layer of tonstein and 2 local layers. The total thickness of these tonsteins is 0.03~0.24 m, with an average of 0.11 m. The coal seam is thinner at the junction of the Xiaoyutuo and Daluo mines, with a thickness of less than 0.75 m. The overall thickness of the coal seam M₇ is 0.71~1.62 m, with an average of 1.11 m. It is a thin coal seam with a simple structure and a stable thickness. In certain regions, the middle part of the coal seam is interspersed with a 0.01~0.57 m thick layer of argillaceous tonstein. The most important recoverable coal seam, M₈, is 0.83~6.43 m thick, with an average thickness of 3.04 m, and is a medium-thickness and stable coal seam. The structure of the coal seam is simple, and the tonsteins are generally located in its upper part, with a total thickness of 0.03~0.58 m and an average thickness of 0.24 m. The thickness of the zone delimiting the lower part of the coal seam is generally 6~9 times that of the upper part, leading to the formation of a three-layer tonstein structure with two coal layers and one tonstein layer. The coal seam M₁₂, situated in the plunging crown of the Yutiao anticline, is located in the area including the coal seams M₁₁ and M₁₂. It is directly overlain by aluminum mudstone, of which the east side is the independent stratification area of the coal seams M₁₁ and M₁₂. The coal seam M₁₁ is located above the coal seam M₁₂, with a thickness of 0.41~3.41 m. The coal seam M₁₁ is partially recoverable, while the coal seam M₁₂ does not have, generally, a recoverable thickness, belonging to a nonrecoverable coal seam. In this study, the two coal seams are jointly referred to as coal seam M₁₂. The total thickness of the coal seam M₁₂ is 0.31~3.33 m, with an average of 0.86 m, indicating that it is a thin coal seam; its general thickness is between recoverable and critically recoverable, making it a relatively stable coal seam.

3. Sampling and Methods

3.1. Evaluation of the Samples

Samples from three CBM wells (QD1, QM1, and QM2 wells) and more than eighty coal exploration boreholes of the Upper Permian Longtan Formation in the Songzao coalfield were collected, with burial depths ranging from approximately 400 to 1700 m, and the distribution of CBM gas in the main coal seams is described. Then, 99 experimental samples of high-rank coal from 3 drilling cores in the QD1, QM1, and QM2 wells and 5 coal exploration boreholes (ZK1, ZK4, SZK8-2, SZK10-3, and SZK10-2) in the coalfield were analyzed in depth. The experimental materials were systematically extracted from the coal seams M₆, M₇, M₈, and M₁₂ of the Longtan Formation to determine geological parameters such as macerals, vitrinite reflectance (R_0), total organic carbon (TOC), amount of free hydrocarbons plus yield of residual hydrocarbons ($S_1 + S_2$), maximum pyrolysis temperature (T_{max}) in rock pyrolysis, pore structure, porosity, and permeability, gas content, and components. All the materials were sealed with desiccators and then measured in the laboratory of the Chongqing Mineral Resources Supervision and Testing Center, Chinese Ministry of Land and Resources. Some data for the coal seams M₆, M₇, M₈, and M₁₂ of the Songzao coalfield, such as thickness, CBM gas content, and macerals, were primarily obtained from previous studies [14,31,33–35,37,40,41] and geological reports on the detailed investigation of coal resources in various coal mines of the coalfield.

3.2. Analytical Methods

In this study, macerals and R_0 were measured using a Leica DM4500P light microscope (Leica, Wetzlar, Germany) with a 40× objective to analyze the volume percentages of macerals and evaluate the thermal maturity of organic matter based on reflectance spectrometry, fluorescence, and transmission spectrometry. The analytical methods referred to the Chinese oil and gas industry standards SY/T 6414-2014 [42] and SY/T 5124-2012 [43]. Five thermal evolution stages could be generally identified, i.e., immature ($R_0 < 0.5\%$),

lowly mature (R_0 , 0.5~0.7%), mature (R_0 , 0.7~1.3%), highly mature (R_0 , 1.3~2.0%), and overmature ($R_0 > 2.0\%$) stages.

To determine the original parent organic matter material in the hydrocarbon source rock, coal samples were pyrolyzed using a China Haicheng Rock-Eval VIII instrument (Haicheng Petrochemical Instrument Factory, Haicheng, China) with a flame ionization detector. The program was carried out in accordance with the national standard GB/T 18602-2012 [44].

The pore structure was observed, and the pores were counted by scanning electron microscopy (SEM) and high-pressure mercury intrusion porosimetry. SEM imaging was performed using an American Thermo Fisher Scientific Apreo SHiVac-Type field-emission scanning electron microscope (FE-SEM) (Thermo Fisher Scientific, Waltham, MA, USA) and an American Gatan 697 Iliion II Argon ion-polishing mill (AMETEK, Berwyn, PA, USA) to determine the pore characteristics in the coal samples based on the Chinese oil and gas industry standard SY/T 5162-2014 [45]. The classification of the pore type referred to a previous work, which described organic matter pores, interparticle mineral pores, intraparticle mineral pores, and fracture pores [46]. Based on the guidelines of the International Union of Pure and Applied Chemistry (IUPAC), pores in coal can be classified into three categories, i.e., “micropores”, with a diameter between 0 and 0.002 μm (0~2 nm), “mesopores” with a diameter between 0.002 μm and 0.05 μm (2~50 nm), and “macropores” with a diameter greater than 0.05 μm (>50 nm) [47]. The mercury intrusion porosimetry was conducted via an American Mike Autopore IV 9500 mercury porosimeter (Micromeritics, Atlanta, GA, USA) to determine different pore volumes under the national standard of GB/T 21650.1-2008 [48].

The porosity and permeability were determined via an American CORETEST SYSTEMS Inc. AP-609 porosity–permeability tester (CoreTest, Atlanta, GA, USA) with the analyzed porosity ranging from 0.1 to 40%, and permeability ranging from 0.001 to 10,000 mD on the basis of the national standard SY/T 6385-2016 [49].

The gas content and its components were determined by in situ gas desorption and isothermal adsorption experiments and gas composition determination. The contour map of CBM gas concentration was established by referring to two geostatistical methods, kriging and triangulation, based on previous research and geological data on coal resources in the Songzao coalfield. The in situ CBM desorption was measured using a self-developed in situ gas-bearing test instrument from the Chongqing Institute of Geology and Mineral Resources to evaluate CBM potential and sweet spot prediction. The in situ test methods referred to the national standard GB/T 19559-2008 [50]. The isothermal adsorption experiment was performed using a ZJ466 Rubotherm IsoSORP HP StaticIII-Type magnetic suspension balance gravimetric high-pressure isothermal adsorption–desorption instrument (Rubotherm, Bochum, Germany). The Langmuir volume pressure is referred to as the Langmuir adsorption isothermal [51]. The gas composition was evaluated by using an ITQ 900 gas chromatographer (GC) (Thermo Fisher Scientific, Waltham, MA, USA) equipped with a thermal conductivity detector and a flame ionization detector based on the national standard GB/T 13610-2014 [52].

4. Results

4.1. Coal Geochemical Characterization

The coal geochemical parameters were directly obtained from the maceral, rock pyrolysis, and R_0 experiments. The coal maceral analysis of samples from the Datong mine and the QD1 well revealed that the average content of organic components in the coal seams M_7 , M_8 , and M_{12} was 81.5 to 88.0%, with the coal seam M_8 having the highest content (Table 2). The content of typical inorganic components varied from 12.0 to 18.5%, with the coal seam M_{12} possessing the highest content. On average, vitrinite was found to contribute 60.1–69.0% of the organic components, whereas inertinite accounted for 14.3–25.3% of them. Clay minerals appeared to be the most abundant inorganic component, followed by sulfide minerals, while oxide and carbonate minerals were less prevalent.

Table 2. Coal macerals from the Datong mine and the QD1 well.

Coal Seam Number	Coal Macerals from Main Coal Seams							(<u>Minimum~maximum</u>)
	Organic Component			Inorganic Component				Average (quantity)
	Vitrinite (%)	Inertinite (%)	Subtotal (%)	Clay Mineral (%)	Sulfide Mineral (%)	Oxide Mineral (%)	Carbonate Mineral (%)	Subtotal (%)
M ₇	<u>55.2~64.3</u> 60.1 (5)	<u>19.3~34.2</u> 25.3 (5)	<u>81.8~89.4</u> 85.4 (5)	<u>5.6~13.8</u> 9.7 (5)	<u>1.1~4.9</u> 2.5 (5)	<u>0.7~1.8</u> 1.1 (5)	<u>0.4~2.2</u> 1.3 (5)	<u>13.9~18.2</u> 14.6 (5)
M ₈	<u>60.3~77.1</u> 69.0 (7)	<u>10.5~25.6</u> 19.0 (7)	<u>85.6~90.3</u> 88.0 (7)	<u>3.3~9.8</u> 7.6 (7)	<u>1.2~5.2</u> 2.5 (7)	<u>0.1~5.8</u> 1.6 (7)	<u>0.1~0.6</u> 0.3 (7)	<u>9.7~14.4</u> 12.0 (7)
M ₁₂	<u>62.3~72.2</u> 67.2 (5)	<u>11.0~18.3</u> 14.3 (5)	<u>75.6~85.5</u> 81.5 (5)	<u>8.7~16.3</u> 12.5 (5)	<u>2.0~7.1</u> 4.1 (5)	<u>0.1~1.5</u> 0.4 (5)	<u>0.1~3.7</u> 1.5 (5)	<u>14.5~24.4</u> 18.5 (5)

The four coal samples from the coal seams M₆, M₇, M₈, and M₁₂ in the QD1 well had high TOC contents ranging from 31.49 to 51.32 wt% (Table 3). These studied coals presented low S₁ and S₂ values in the ranges of 0.0916~0.12 mg/g and 4.3565~8.4797 mg/g, respectively. The TOC and S₁ + S₂ values indicated that the coals are overmature, as discussed below, and have a fair hydrocarbon generation potential. The T_{max} values ranged from 534 to 549 °C, with an average of 539 °C, suggesting that the coals experienced thermal evolution to overmaturation. The hydrogen index (HI) values ranged from 13.83 to 16.52 mg HC/g TOC, with a mean value of 15.21 mg HC/g TOC, indicating that type III kerogen (less than 200 mg HC/g TOC) is dominant in the coal seams M₆, M₇, M₈, and M₁₂ of the Longtan Formation. The R₀ values varied from 2.09 to 2.24%, averaging 2.17%. In addition, the coals in the Longtan coal measure strata from Chongqing city contain mostly semianthracite and anthracite, with R₀ values of 1.88~2.6% on average, according to previous studies [14,29,31], and underwent a highly thermal evolution process, leading to high-rank coal with a post-thermal maturity and good potential for CBM accumulation.

Table 3. Geochemical parameters of the high-rank coal in the QD1 well.

Coal Seam Number	S ₁ (mg/g)	S ₂ (mg/g)	T _{max} (°C)	HI (mg/g)	TOC (wt%)	R ₀ (%)
M ₆	0.0975	7.183	534	15.66	45.86	2.13
M ₇	0.12	8.4797	535	16.52	51.32	2.09
M ₈	0.0916	7.3502	535	14.81	49.63	2.24
M ₁₂	0.1047	4.3565	549	13.83	31.49	2.2

Remarks: HI = S₂ × 100/TOC, mg HC/g TOC.

4.2. Coal Reservoir Characterization

4.2.1. Pore Structure

The coal samples from the coal seams M₆, M₇, M₈, and M₁₂ analyzed by SEM showed that the coal pores were mainly gas holes and erosion pores, which were distributed inside the massive organic components. These pores' diameters were generally 0.13~3.45 μm, with a maximum of 10.69 μm (Figure 4). Coal fissures had not developed, and only a few of them were visible. The width of these fissures was generally 1.0~7.18 μm. The fissures were mainly shell-like and step-shaped. The organic components were distributed in flatter blocks and strips, with clastic, agglomerate, and granular clay minerals dominating the mineral composition of the coal.

The coal pore volumes in the study area varied from 1.48 to 48.40 × 10⁻⁴ cm³/g, with an average of 10.86 × 10⁻⁴ cm³/g, and the average volume ratio was 33.33% (Table 4). Meanwhile, the volume ratio of the coal seam M₆ was more than 40%, and micropores were predominant. The variation range of the micropore volumes was 2.34~48.40 × 10⁻⁴ cm³/g, with an average of 11.78 × 10⁻⁴ cm³/g, and the average volume ratio of the micropores was 32.28%. The variation range of the mesopore volume was 1.48~11.40 × 10⁻⁴ cm³/g, with an average of 4.56 × 10⁻⁴ cm³/g. The volume ratio of the mesopores was 7.22~20.11%, with an average of 13.59%. The mesopore volume in these coal seams was much smaller. Moreover, the variation range of the macropore volumes was 7.87~27.24 × 10⁻⁴ cm³/g, with an average of 16.22 × 10⁻⁴ cm³/g, and the volume ratio of the macropores ranged from 28.12 to 81.37%, with an average of 54.14%. In summary, the coal in the coalfield appeared to contain mainly macropores and micropores, and their total proportion was greater than 80%. Among them, the coal seam M₆ revealed a prevalence of micropores, and the other coal seams presented a prevalence of macropores.

4.2.2. Porosity and Permeability

Depending on the porosity and permeability data of 19 coal samples from different mines within the coalfield, it was determined that the coal porosity ranged from 2.36% to 5.26%, with an average of 4.29%. The permeability varied from 0.0029 to 0.0221 mD, with the majority of the samples having a permeability below 0.01 mD and an average

permeability of 0.0069 mD and thus placed in the ultralow-permeability coal seam group (Table 5). Except for the QM1 well, the coal permeability in the Daluo and Shihao mines was found to be extremely low, with the highest permeability not exceeding 0.01 mD, and the average being 0.006 mD, which is related to the fact that the tested coal samples were taken from deep coal seams (buried more than 1000 m).

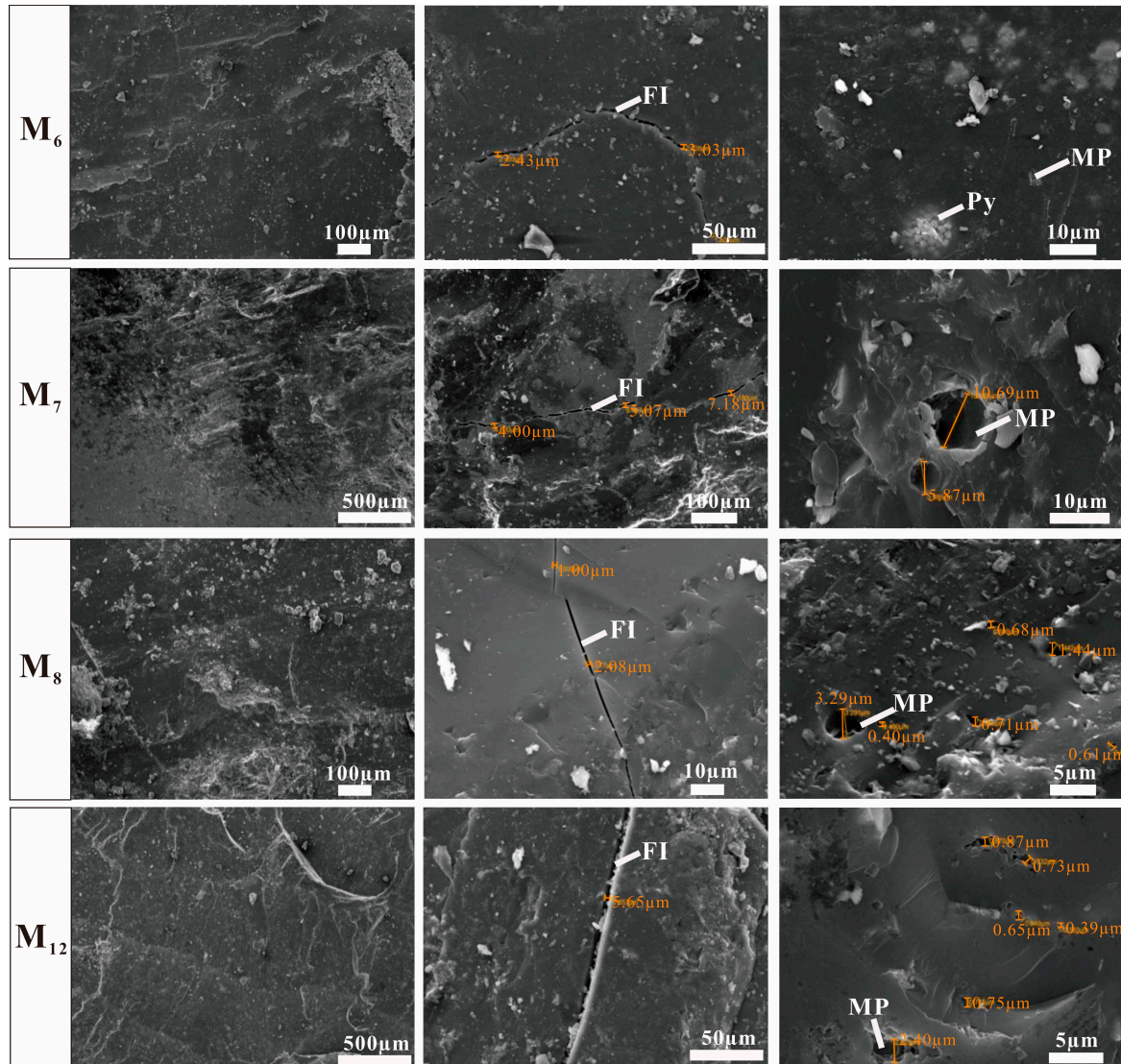


Figure 4. Microstructural photographs of coal from the coal seams M_6 , M_7 , M_8 , and M_{12} . FI, fissure; MP, macroscopic pore; Py, pyrite.

Table 4. Coal pore structure and volume parameters in the coal seams M_6 , M_7 , M_8 , and M_{12} determined by mercury injection porosimetry.

Coal Seam Number	Buried Depth (m)	Pore Volume ($10^{-4}\text{cm}^3/\text{g}$)				Pore Volume Ratio (%)			Well/Borehole Number
		V1	V2	V3	Vt	V1/Vt	V2/Vt	V3/Vt	
M_6	886.20	7.87	3.47	8.56	19.90	39.55	17.44	43.02	QM1 Well
	1661.85	11.12	6.43	22.00	39.55	28.12	16.26	55.56	Daluo Mine, ZK1
	1381.45	15.29	6.99	20.30	42.58	35.91	16.42	47.67	Daluo Mine, ZK4
	912.41	15.32	5.16	13.70	34.18	44.82	15.10	40.08	Shihao Mine, SZK8-2
	1074.34	25.22	11.40	48.40	85.02	29.66	13.41	56.93	Shihao Mine, SZK10-2
	1444.85	19.75	6.89	15.50	42.14	46.87	16.35	36.78	Shihao Mine, SZK10-3

Table 4. Cont.

Coal Seam Number	Buried Depth (m)	Pore Volume ($10^{-4}\text{cm}^3/\text{g}$)				Pore Volume Ratio (%)			Well/Borehole Number
		V1	V2	V3	Vt	V1/Vt	V2/Vt	V3/Vt	
M ₇	1672.09	15.84	2.23	3.24	21.31	74.33	10.46	15.20	Daluo Mine, ZK1
	1393.31	15.73	2.50	5.98	24.21	64.97	10.33	24.70	Daluo Mine, ZK4
	917.76	14.77	3.32	6.52	24.61	60.01	13.49	26.49	Shihao Mine, SZK8-2
	1452.42	14.39	5.27	6.55	26.20	54.92	20.11	25.00	Shihao Mine, SZK10-3
	1081.12	14.64	3.12	10.00	27.76	52.74	11.24	36.02	Shihao Mine, SZK10-2
	898.70	14.20	3.76	8.05	26.01	54.59	14.46	30.95	QM1 Well
M ₈	1685.02	18.97	2.19	3.54	24.70	76.80	8.87	14.33	Daluo Mine, ZK1
	1400.17	14.54	3.16	9.11	26.81	54.23	11.79	33.98	Daluo Mine, ZK4
	929.95	14.36	3.13	5.37	22.86	62.82	13.69	23.49	Shihao Mine, SZK8-2
	1461.11	16.48	5.19	14.60	36.27	45.44	14.31	40.25	Shihao Mine, SZK10-3
	1091.12	18.45	5.45	14.00	37.90	48.68	14.38	36.94	Shihao Mine, SZK10-2
	905.90	16.68	1.48	2.34	20.50	81.37	7.22	11.41	QM1 Well
M ₁₂	1704.07	10.89	3.50	7.51	21.90	49.73	15.98	34.29	Daluo Mine, ZK1
	1431.64	27.24	2.74	6.32	36.30	75.04	7.55	17.41	Daluo Mine, ZK4
	1114.23	20.42	10.90	24.50	55.82	36.58	19.53	43.89	Shihao Mine, SZK10-2
	934.30	14.76	2.10	3.14	20.00	73.80	10.50	15.70	QM1 Well

Remarks: V1, V2, and V3 are the pore volumes of macropores, mesopores, and micropores, respectively. Vt is the total pore volume.

Table 5. Coal porosity and permeability data of samples from the coal seams M₆, M₇, M₈, and M₁₂.

Coal Seam Number	Burying Depth (m)	Porosity (%)	Permeability (mD)	Well/Borehole Number
M ₆	1662	4.25	0.0063	Daluo Mine, ZK1
	1381	4.32	0.0065	Daluo Mine, ZK4
	1445	3.82	0.0077	Shihao Mine, SZK10-3
	912	4.57	0.0050	Shihao Mine, SZK8-2
	1074	4.67	0.0063	Shihao Mine, SZK10-2
	899	2.36	0.0221	QM1 Well
M ₇	1672	5.01	0.0062	Daluo Mine, ZK1
	1393	3.95	0.0054	Daluo Mine, ZK4
	918	5.08	0.0059	Shihao Mine, SZK8-2
	1452	4.68	0.0086	Shihao Mine, SZK10-3
	1081	3.54	0.0072	Shihao Mine, SZK10-2
	1685	3.95	0.0043	Daluo Mine, ZK1
M ₈	930	5.26	0.0068	Shihao Mine, SZK8-2
	1461	4.16	0.0094	Shihao Mine, SZK10-3
	1091	4.19	0.0031	Shihao Mine, SZK10-2
	1400	3.94	0.0050	Daluo Mine, ZK4
M ₁₂	1704	4.31	0.0075	Daluo Mine, ZK1
	1432	4.21	0.0042	Daluo Mine, ZK4
	1114	5.18	0.0029	Shihao Mine, SZK10-2

4.3. Coal Gas-Bearing Properties

4.3.1. Composition of CBM

According to the gas component data of the 15 coal samples from the QD1, QM1, and QM2 wells (Table 6), the concentration of desorbed CH₄ in the coal seams M₆, M₇, M₈, and M₁₂ ranged from 88.62 to 99.41%, with an average of 94.45%. The content of C²⁺ was 0~0.18%, while the inorganic component comprised minor amounts of CO₂ and N₂. The CO₂ content ranged from 0.48 to 1.55%, while the N₂ content was typically less than 9.71%.

4.3.2. Distribution of the CBM Gas Contents

Based on the in situ desorption analysis of the CBM gas content in the QM1, QM2, and QD1 wells, the in situ desorption gas contents in the coal seams M₆, M₇, M₈, and M₁₂ were 12.5~15.3 m³/t, 21.4~25.8 m³/t, 15.9~25.6 m³/t, and 12.1~21.1 m³/t, respectively. The gas contents in the main coal seams from the three CBM wells were more than 8.0 m³/t, indicating a good material foundation for gas generation. Meanwhile, vertically, the gas

contents in the coal seams M₇ and M₈ were relatively higher than those in the coal seams M₆ and M₁₂.

Table 6. Gas component data of samples from the coal seams M₆, M₇, M₈, and M₁₂ in the QD1, QM1 and QM2 wells.

Well Number	Coal Seam Number	Content without Air of Components (Volume)/%			
		N ₂	CO ₂	CH ₄	C ²⁺
QD1 Well		6.90	0.88	92.18	0.04
QM1 Well	M ₆	2.56	1.12	96.21	0.11
QM2 Well		7.81	0.90	91.12	0.18
QM2 Well		1.51	0.90	97.44	0.16
QM1 Well	M ₇	9.54	0.65	89.71	0.10
QD1 Well		6.26	0.89	92.84	0.01
QM1 Well		6.72	1.05	92.15	0.08
QM1 Well	M ₈	0.00	0.50	99.41	0.09
QM2 Well		9.71	1.55	88.62	0.13
QM2 Well		8.69	1.24	89.92	0.15
QM2 Well		2.08	1.24	96.50	0.18
QD1 Well	M ₁₂	3.72	1.23	95.05	0.00
QM2 Well		1.21	0.83	97.74	0.23
QM2 Well		0.45	0.53	98.85	0.17
QM1 Well		0.35	0.48	99.03	0.13

As can be seen from the distribution of the CBM gas contents in the coal seams M₆, M₇, M₈, and M₁₂ from different mines (Figure 5 and Table 7), the average CBM gas content in these coal seams in the Xiaoyutuo mine ranged from 12.47 to 21.45 m³/t, with the highest content was found in the coal seam M₈. The average CBM gas contents in the coal seams of the Datong and Shihao mines showed a very similar variation trend and were only 11.99~16.98 m³/t and 11.15~17.42 m³/t, respectively. The average CBM gas content in the coal seams of the Daluo mine ranged from 26.14 to more than 30 m³/t and was the highest in the study area.

Table 7. Average CBM gas contents of the coal seams M₆, M₇, M₈, and M₁₂ in different coal mines of the Songzao coalfield.

Coal Mine	Coal Seam	Average Depth (m)	Average Gas Content (m ³ /t)
Xiaoyutuo	M ₆	776.98	12.47
	M ₇	850.29	15.42
	M ₈	918.95	21.45
	M ₁₂	1057.1	18.14
Datong	M ₆	533.39	11.99
	M ₇	640.27	15.92
	M ₈	690.34	16.98
Daluo	M ₇	1152.59	26.14
	M ₈	1549.19	26.25
	M ₁₂	1587.06	28.18
Shihao	M ₆	885.48	11.17
	M ₇	1025.49	17.42
	M ₈	1076.72	17.02
	M ₁₂	1079.65	11.51

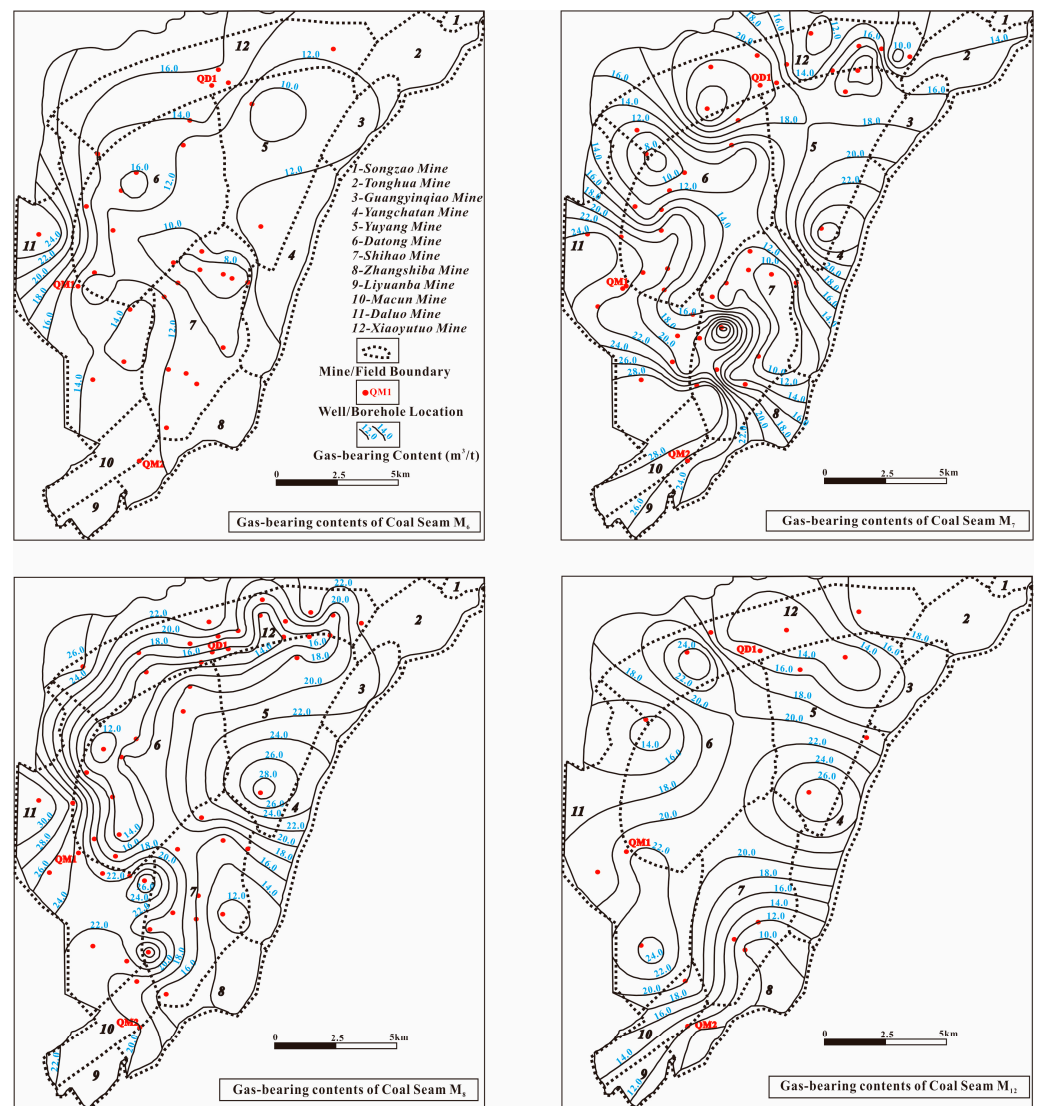


Figure 5. Regional distribution of the CBM gas contents in high-rank coal from the coal seams M_6 , M_7 , M_8 , and M_{12} . Typical CBM gas content data are reported in Table S1.

The average CBM gas content in the coal seam M_8 in the coalfield was usually higher than $16 \text{ m}^3/\text{t}$, and some areas with lower gas contents were found only at the junction of the Datong, Xiaoyutuo, and Daluo mines and at the junction of the Datong and Shihao mines. The highest CBM gas content in regional coal seams was above $30 \text{ m}^3/\text{t}$, and these high-content sites are mainly distributed in deep areas of the Xiaoyutuo, Daluo, and Shihao mines along the Yutiao anticline. The total CBM gas content in these coal seams appeared to increase from east to west and as the elevation of the coal seam floor decreased.

4.3.3. Adsorption–Desorption Characteristics

The isothermal adsorption results of CBM gas analysis revealed that the Langmuir volume and the Langmuir pressure in the coal seam M_6 were $6.40 \text{ cm}^3/\text{g}$ and 1.30 MPa , respectively (Figure 6). The coal seam M_8 was characterized by the largest Langmuir volume of $24.88 \text{ cm}^3/\text{g}$ and a Langmuir pressure of 1.04 MPa . The Langmuir volume of the coal seam M_{12} was $15.24 \text{ cm}^3/\text{g}$, and its Langmuir pressure was only 0.91 MPa .

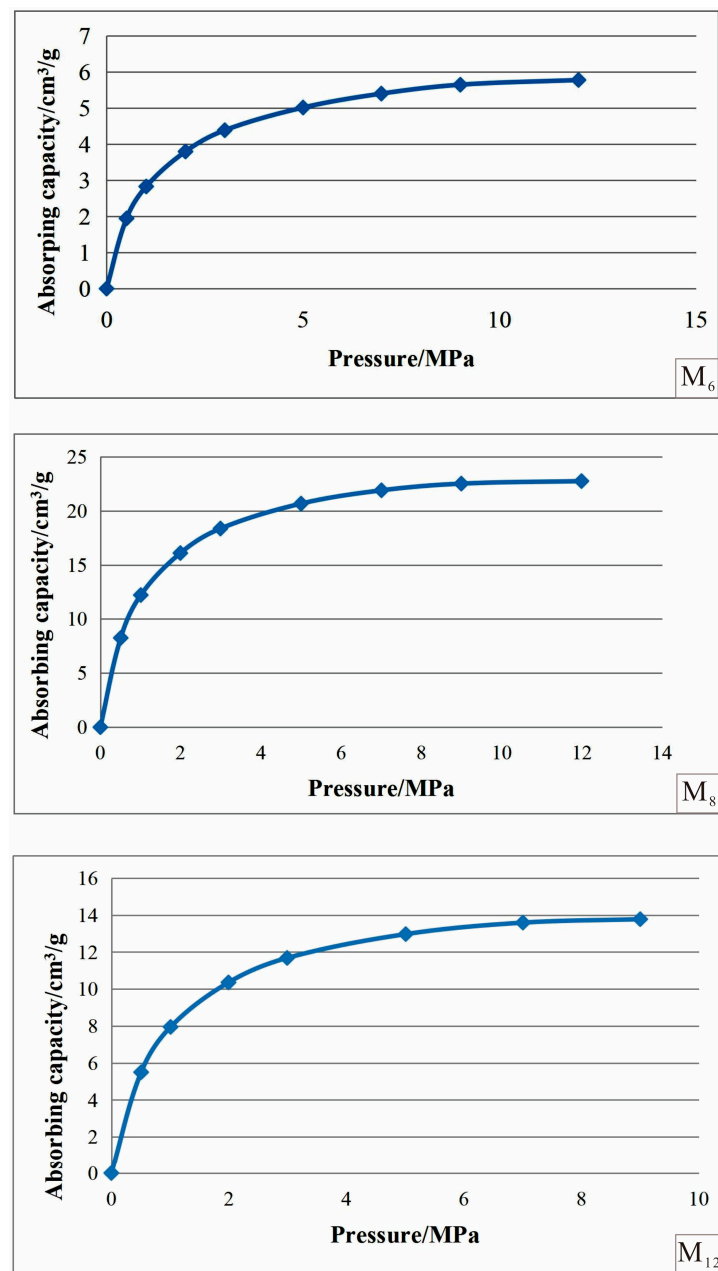


Figure 6. Isothermal adsorption data of CBM gas in the coal seams M₆, M₈, and M₁₂ from the QD1 well.

The central depths (vertical depths) of the coal seams M₆, M₈, and M₁₂ in the QD1 well were 888.1 m, 904.7 m, and 933.6 m, respectively. Based on the formation pressure coefficient of 1.0 for the Xiaoyutuo mine, the formation pressures of the coal seams M₆, M₈, and M₁₂ were 8.88 MPa, 9.05 MPa, and 9.34 MPa, respectively. Combining these data with the isothermal adsorption curve of the coal samples and the Langmuir isothermal adsorption equation, the theoretical CBM gas contents of the coal seams M₆ and M₁₂ were 5.58 m³/t and 13.88 m³/t, respectively. However, the coal seam M₈ showed the highest theoretical gas content of 22.32 m³/t, appearing as the most promising candidate for CBM exploration and development efforts.

5. Discussion

5.1. Constraint of the Depositional Environment on Coal Formation

The depositional environment constrains the characteristics of coal accumulation, the petrographic composition, and the spatial combinations of coal seams [14,31,53–55], which largely provide the material basis for CBM generation. When the depositional conditions are good, the coal seam thickness is large, and its distribution is stable, leading to a significant possibility of CBM gas production. In contrast, when the subsidence amplitude is not obvious, and the depositional conditions are poor, the coal seam thickness is unevenly distributed, and CBM gas production may also be relatively small.

A set of lowland residual plain deposits, dominated by bauxitic mudstone and kaolinite tonstein, developed steadily and were widely distributed throughout the weathering and denudation substrate at the top of the Maokou Formation during the early Wuchiapingian Period in the Songzao coalfield, as the crust started to sink slowly, and a large-scale sea recession stopped (Figures 2 and 7a,b).

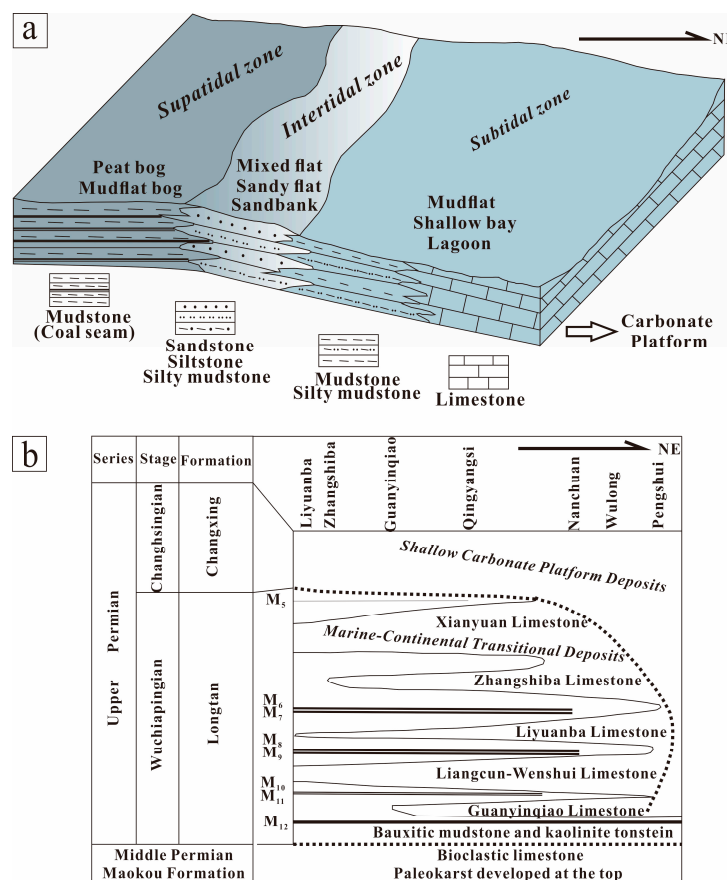


Figure 7. (a) Horizontal Wuchiapingian depositional pattern in the Songzao coalfield; (b) longitudinal Wuchiapingian depositional system of the Songzao coalfield.

As the crust continued to sink, and the first transgression invaded the area from the northeast to the southwest of Chongqing, the range of the marine–continental transitional zone gradually expanded, and large-scale coal accumulation occurred throughout the coalfield, resulting in the formation of the stably developed coal seam M₁₂, which is the product of regional transgression and is commonly presented during the initial stage of the early Wuchiapingian Period.

After that, seawater continued to rise slowly, the effect of coal gathering ended, the littoral tidal flat environment began to develop in a large region, and a set of fine clastic sediments such as siltstone and silty mudstone generally formed. Meanwhile, under the dual effects of further crust sinking and seawater rising, marine carbonate sediments

appeared locally in the coalfield, and a thicker layer of limestone formed, represented by the Guanyinqiao limestone, which was deposited in a shallow bay with varying amounts of siliceous clastics. As the transgression stopped briefly, and the crust rose slowly, tidal flat and lagoon deposits developed on the top of the Guanyinqiao limestone, consisting primarily of sandstone, shale, and mudstone, locally interspersed with thin layers of limestone and unstable coal seams such as the coal seams M₁₀ and M₁₁. The largest transgression of the Wuchiapingian Period occurred after the deposition of the coal seams M₁₀ and M₁₁, forming the Wenshui–Liangcun limestone of the shallow bay environment throughout the whole coalfield. The Wenshui–Liangcun limestone represents the highest position of the transgression during the Wuchiapingian Period, and then the depositional sequence of lagoon and tidal flat redeveloped due to a seawater falling trend toward the east side of the coalfield and a crustal basement imbalance, forming the coal seam M₇, which also reflects the fluctuating in and out movement of seawater. During this stage, the coal seams M₈ and M₉ with regional spreading also formed, among which the coal seam M₈ is the best developed.

With the beginning of a new transgression, the crust sank, and seawater rose, and the depositional sequence shallow bay–lagoon–tidal flat manifested again over a wide range, forming fine clastic sediments dominated by siltstone and silty mudstone, thin coal seams (the relatively stable coal seams M₆ and M₇), and thin marker limestone layers (the Liyuanba, Zhangshiba, and Xianyuan limestone layers). During this stage, there were several short periods of regression, and the coal measure strata better developed to the west side of the coalfield. By the Changhsingian Period, a long-term and stable shallow carbonate platform had emerged in the Songzao field, implying the end of the Wuchiapingian marine–continental transitional environment.

However, the interpretation of the attributes of sparse vertical and horizontal sections and of borehole data using a geologic model, due to the heterogeneity and the inability to explain their spatial distribution, is difficult [56]. The traditional geostatistical interpolation approaches identified unhandled uncertainty in the Wuchiapingian marine–continental transitional environment pattern. This issue can be overcome by incorporating supplemental testing data to obtain more accurate inference results using hybrid techniques, such as a hybrid ensemble-based automated deep learning methodology [56]. In conclusion, the Songzao coalfield experienced repeated transgression and regression events from northeast to southwest throughout the Late Permian Wuchiapingian Period, with shallow bay–tidal flat–lagoon deposits dominating the depositional system (Figure 7a,b). Large-scale and stable coal accumulation mainly occurred in the early and middle Wuchiapingian. After the progressive rising of seawater and the variable fluctuation of the crust, no favorable coal-forming environment developed; hence, few coal seams formed in the coalfield in the middle to late Wuchiapingian.

5.2. Tectono-Thermal Evolution Constraining the CBM Production Potential

The Emeishan mantle plume activity was a large-scale tectono-thermal evolution event in Southwest China that constructed the Emeishan large igneous province in the latest middle Permian [57–59], triggering multistage intermediate-acidic volcanic eruptions during the late Permian Wuchiapingian and Changhsingian [60–62]. This event, with different development stages (emplacement, doming, and erosion of the Emeishan mantle plume and continued volcanism), deeply impacted the marine sedimentary strata in this time interval, forming a high geothermal field [63–67]. The Dongwu movement between the middle and the late Permian was a rapid differential uplift of the crust caused by mantle plume activity, and the top of the middle Permian Maokou Formation exposed at the surface underwent weathering and denudation [38]. The resulting tectonic fractures, such as the Huayingshan and Qiyueshan fault belts, provided migration channels for magmatic upwelling, intrusion, and volcanic activity throughout some regions of Sichuan province and Chongqing city in Southwest China (Figure 8a,b).

As the crust subsided again, marine–continental transitional deposits began to develop during the late Permian Wuchiapingian Period, forming the coal measure strata of the Longtan Formation. In addition, some tonstein (or tuff) layers were found near or within the coal seams of the Longtan Formation in southern Sichuan province, southern Chongqing city, western Guizhou province, and eastern Yunnan province ([33,35,36,68–70] and Figure 2), which belong to the outer zone of the Emeishan large igneous province and resulted from the waning activity of the mantle plume (Figure 8a,b). The tonsteins (or tuffs), originating from various partial melting conditions, indicated that the volcanic activities were characterized by multiple eruptions, relatively short time intervals, and small scales during peat accumulation. These geological conditions ensured the required temperature and time for the overmaturation and the achievement of the corresponding thermal metamorphic degrees of the whole coal seams in the Longtan Formation. Multistage volcanic eruptions during the late Permian could have resulted in pronounced increases in the geothermal gradient and heat flow [62,64,67,71,72], promoting the thermal metamorphism of the coal seams and accelerating CBM gas formation.

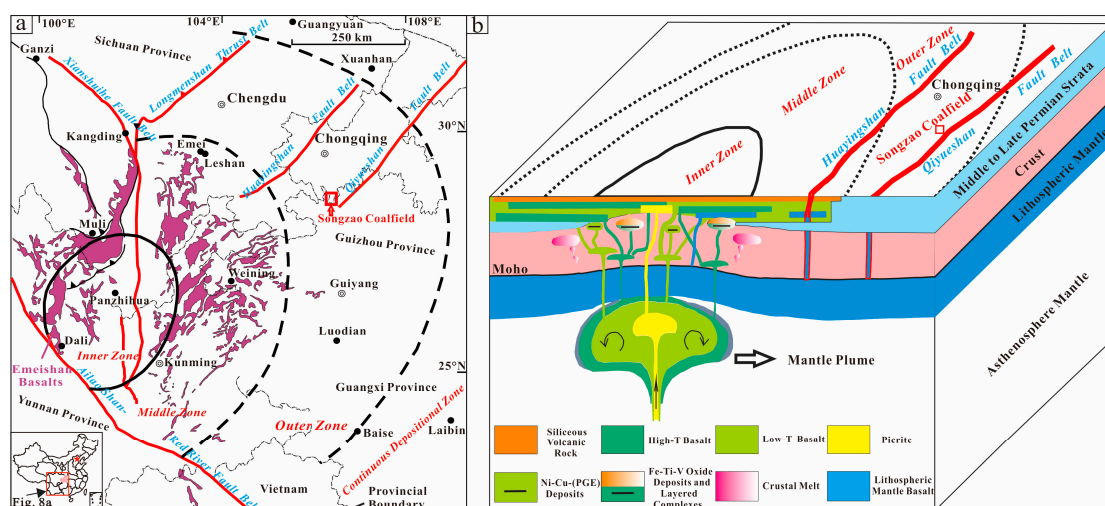


Figure 8. (a) Distribution of the Emeishan large igneous province showing the location of the Songzao coalfield, modified after [73]; (b) middle–late Permian magmatic and tectonic–thermal responses to the Emeishan large igneous province, modified after [59,65].

The reconstructed heat flow history modeling of the Emeishan large igneous province region based on multiple paleogeothermal parameters indicated a high heat flow of 80–110 mW/m² in the late Permian. The Longtan coal measure strata of the coalfield are located within the region ([63,66] and Figure 8a,b), which could be viewed as direct evidence of temperature anomalies related to mantle plume activity. Furthermore, thermal metamorphism at higher temperatures could also change the molecular composition of coal, resulting in an increase in the degree of coal metamorphism (high-rank coal) and vitrinite reflectivity (1.88–2.14%). Thermal metamorphism may also lead to increases in the local CBM pore volume (including gas hole and erosion pore numbers inside organic components) and gas content, producing a huge amount of pyrolytic methane adsorbed in the coal seams and further enhancing the gas production potential in high-rank coals.

5.3. Effect of the Regional Geological Structure on CBM Accumulation

The influence of regional geological structures on the CBM gas content is generally significant. The structure may not only influence the folding, twisting, shape change, fracture dislocation, and interbed sliding of coal seams [11,74,75], but also cause the escape and redistribution of CBM stored in coal reservoirs, affecting the gas content in coal seams in different structural sites [12,76,77]. In the Yuyang and Yangchatan mines of the Songzao coalfield, several tiny reverse and normal faults have developed underground (Figure 1).

Meanwhile, there is not much variation between the thickness of the coal seams M_6 , M_7 , M_8 , and M_{12} of the Permian Longtan Formation in the two mines (Figure 3). However, the CBM gas contents in the main coal seams in the Yuyang mine are significantly lower than those in the Yangchatan mine (Figure 5). This implies that CBM is easily discharged, and the gas content in the coal seams frequently decreases significantly in underground tension fractures in the Yuyang mine. Nevertheless, in the Yangchatan mine, underground compression fractures can effectively close and collect CBM, and the gas content in the coal seams increases as the formation pressure increases. Few underground faults developed in the other 10 mines of the Songzao coalfield, although the distribution of the CBM gas content in the coal seams M_6 , M_7 , M_8 , and M_{12} has nearly always a certain regularity. For instance, the coal seam M_8 has a thickness of only 0.33 m at the plunging crown of the Yutiao anticline, yet abundant tectonic coals developed inside it, with a CBM gas content of up to $32.77 \text{ m}^3/\text{t}$. Furthermore, the CBM gas content of the coal seam M_8 was found to be more than $15 \text{ m}^3/\text{t}$ in the trap areas of the Yutiao and Yangchatan anticlines, such as the Datong and Shihao mines. The coal seams of the adjacent Zhangshiba and Liyuanba mines are monoclinic, with thickness ranging from 3.5 to 6.0 m. The gas content in the coal seam M_8 normally fell between 12 and $20 \text{ m}^3/\text{t}$. Moreover, the gas content in the coal seam M_8 was found to increase as the formation pressure rose in the northern and southern compound structural areas at the plunging convergence site between the Lianghekou syncline and the Yangchatan anticline, i.e., in the northern part of the Guanyinqiao mine, the southern part of the Tonghua mine, and the southern parts of the Yangchatan and Shihao mines (Figure 6). This case illustrates that whether the fold structure is enclosed is the most critical element influencing variances in the lateral distribution of the CBM gas content. Tectonic coals are very developed in the Songzao coalfield, with a high CBM gas content in strongly folded areas or tightly bonded areas, such as the plunging crown of an anticline and the trap area between two anticlines, destroying the original pores and fissures of coal seams and increasing the CBM gas content to a high degree in certain enclosed areas.

6. Conclusions

- (1) The high-rank coals in the coal seams M_6 , M_7 , M_8 , and M_{12} of the Permian Longtan Formation from the Songzao coalfield have high vitrinite and TOC contents (60.1~69.0%, 31.49~51.32 wt%), high T_{\max} and R_0 values (averaging $539 \text{ }^\circ\text{C}$, 2.17%), low HI values (averaging 15.21 mg HC/g TOC), high porosity and low permeability, and comparatively high gas contents.
- (2) The frequent changes among shallow bay, tidal flat, and lagoon depositional environments triggered the formation of multiple coal seams and furnished the material basis for CBM generation. The multistage tectono-thermal evolution caused by the Emeishan mantle plume activity provided favorable temperatures and the necessary time for the overmaturation and thermal metamorphism of the coal seams and the acceleration of pyrolytic CBM formation.
- (3) The effective regional structures, such as the enclosed fold regions like the plunging crown of the anticline and the trap area between two anticlines, directly optimized the conditions for CBM enrichment in the high-rank coals.

Supplementary Materials: The following supporting information can be downloaded at: <https://www.mdpi.com/article/10.3390/en17051262/s1>, Table S1: Typical average CBM gas contents in different coal seams from boreholes in the Songzao coalfield.

Author Contributions: Conceptualization, D.C., X.T. and J.W.; methodology and data curation, Y.Z. and C.Z.; formal analysis and investigation, D.G.; writing—original draft preparation, D.C.; writing—review and editing, X.T.; funding acquisition, D.C. and X.T. All authors have read and agreed to the published version of the manuscript.

Funding: This study was supported by the Natural Science Foundation of Chongqing (CSTB2022NSCQ-MSX1221), the National Natural Science Foundation of China (42302027), and the Research Project of SINOPEC East China Company (34600000-23-ZC0611-0003).

Data Availability Statement: All data are contained within the manuscript.

Acknowledgments: We would like to thank the two anonymous reviewers for their valuable comments and constructive suggestions that helped to improve the original quality of this paper.

Conflicts of Interest: The authors declare no conflicts of interest.

References

1. Zhu, Q.Z.; Yang, Y.H.; Zuo, Y.Q.; Song, Y.; Guo, W.; Tang, F.; Ren, J.; Wang, G. On the scientific exploitation of high-rank CBM resources. *Nat. Gas Ind. B* **2020**, *7*, 403–409. [\[CrossRef\]](#)
2. Sang, S.X.; Han, S.J.; Liu, S.Q.; Zhou, X.Z.; Li, M.X.; Hu, Q.J.; Zhang, C. Comprehensive study on the enrichment mechanism of coalbed methane in high rank reservoirs. *J. China Coal Soc.* **2022**, *47*, 388–403, (In Chinese with English Abstract). [\[CrossRef\]](#)
3. Zhu, Q.Z. Improving the production efficiency of high rank coal bed methane in the Qinshui Basin. *Nat. Gas Ind. B* **2022**, *9*, 477–486. [\[CrossRef\]](#)
4. Shao, L.Y.; Hou, H.H.; Tang, Y.; Lu, J.; Qiu, H.J.; Wang, X.T.; Zhang, J.Q. Selection of strategic replacement areas for CBM exploration and development in China. *Nat. Gas Ind. B* **2015**, *2*, 211–221. [\[CrossRef\]](#)
5. Zou, C.N.; Yang, Z.; Huang, S.P.; Ma, F.; Sun, Q.P.; Li, F.H.; Pan, S.Q.; Tian, W.G. Resource types, formation, distribution and prospects of coal-measure gas. *Pet. Explor. Dev.* **2019**, *46*, 433–442. [\[CrossRef\]](#)
6. Qin, Y. Strategic thinking on research of coal measure gas accumulation system and development geology. *J. China Coal Soc.* **2021**, *46*, 2387–2399, (In Chinese with English Abstract). [\[CrossRef\]](#)
7. Li, Y.; Pan, S.P.; Ning, S.Z.; Shao, L.Y.; Jing, Z.H.; Wang, Z.S. Coal measure metallogeny: Metallogenic system and implication for resource and environment. *Sci. China Earth Sci.* **2022**, *65*, 1211–1228. [\[CrossRef\]](#)
8. Tang, S.L.; Tang, D.Z.; Xu, H.; Tao, S.; Li, S.; Geng, Y.G. Geological mechanisms of the accumulation of coalbed methane induced by hydrothermal fluids in the western Guizhou and eastern Yunnan regions. *J. Nat. Gas Sci. Eng.* **2016**, *33*, 644–656. [\[CrossRef\]](#)
9. Qin, Y.; Moore, T.A.; Shen, J.; Yang, Z.B.; Shen, Y.L.; Wang, G. Resources and geology of coalbed methane in China: A review. *Int. Geol. Rev.* **2017**, *60*, 777–812. [\[CrossRef\]](#)
10. Bi, C.Q.; Zhang, J.Q.; Shan, Y.S.; Hu, Z.F.; Wang, F.G.; Chi, H.P.; Tang, Y.; Yuan, Y.; Liu, Y.R. Geological characteristics and co-exploration and co-production methods of Upper Permian Longtan coal measure gas in Yangmeishu syncline, western Guizhou Province, China. *China Geol.* **2020**, *3*, 38–51, (In Chinese with English Abstract). [\[CrossRef\]](#)
11. Cao, D.Y.; Ning, S.Z.; Guo, A.J.; Li, H.T.; Chen, L.M.; Liu, K.; Tan, J.Q.; Zheng, Z.H. Coalfield structure and structural controls on coal in China. *Int. J. Coal Sci. Technol.* **2020**, *7*, 220–239. [\[CrossRef\]](#)
12. Liu, D.M.; Jia, Q.F.; Cai, Y.D.; Gao, C.J.; Qiu, F.; Zhao, Z.; Chen, S.Y. A new insight into coalbed methane occurrence and accumulation in the Qinshui Basin, China. *Gondwana Res.* **2022**, *111*, 280–297. [\[CrossRef\]](#)
13. Sang, S.X.; Zheng, S.J.; Yi, T.S.; Zhao, F.P.; Han, S.J.; Jia, J.L.; Zhou, X.Z. Coal measures superimposed gas reservoir and its exploration and development technology modes. *Coal Geol. Explor.* **2022**, *50*, 13–21, (In Chinese with English Abstract). [\[CrossRef\]](#)
14. Cheng, J.; Li, D.H.; Liu, D.; Yao, G.H.; Ren, S.C.; Li, C.L.; Zhang, L.H.; Tang, B.F. *Coal-Forming Pattern and Quantitative Forecast of the Coal Resources in the Chongqing City*; China University of Geosciences Press: Wuhan, China, 2015; 282p. (In Chinese)
15. Zhu, Q.Z.; Zuo, Y.Q.; Yang, Y.H. How to solve the technical problems in the CBM development: A case study of a CMB gas reservoir in the southern Qinshui Basin. *Nat. Gas Ind. B* **2015**, *35*, 106–109. [\[CrossRef\]](#)
16. Li, Z.T.; Liu, D.M.; Ranjith, P.G.; Cai, Y.D. Geological controls on variable gas concentrations: A case study of the northern Gujiao Block, northwestern Qinshui Basin, China. *Mar. Pet. Geol.* **2018**, *92*, 582–596. [\[CrossRef\]](#)
17. Liang, J.T.; Huang, W.H.; Wang, H.L.; Blum, M.J.; Chen, J.; Wei, X.L.; Yang, G.Q. Organic geochemical and petrophysical characteristics of transitional coalmeasure shale gas reservoirs and their relationships with sedimentary environments: A case study from the Carboniferous-Permian Qinshui Basin, China. *J. Pet. Sci. Eng.* **2020**, *184*, 106510. [\[CrossRef\]](#)
18. Zhu, Q.Z. *New Technologies and Practice of Exploration and Development for High-Rank Coal Bed Methane*; Petroleum Industry Press: Beijing, China, 2021; 268p. (In Chinese)
19. Jiang, W.P.; Zhang, P.H.; Li, D.D.; Li, Z.C.; Wang, J.; Duan, Y.N. Reservoir characteristics and gas production potential of deep coalbed methane: Insights from the no. 15 coal seam in shouyang block, Qinshui Basin, China. *Unconv. Resour.* **2022**, *2*, 12–20. [\[CrossRef\]](#)
20. Cao, L.; Yao, Y.; Cui, C.; Sun, Q. Characteristics of in-situ stress and its controls on coalbed methane development in the southeastern Qinshui Basin, North China. *Energy Geosci.* **2020**, *1*, 69–80. [\[CrossRef\]](#)
21. Zhang, P.; Ya, M.; Liu, C.; Guo, Y.; Yan, X.; Cai, L.M.; Cheng, Z. In-situ stress of coal reservoirs in the Zhengzhuang area of the southern Qinshui Basin and its effects on coalbed methane development. *Energy Geosci.* **2023**, *4*, 100144. [\[CrossRef\]](#)
22. Yang, Y.; Li, X.; Zhang, Y.; Mei, Y.; Ding, R. Insights into moisture content in coals of different ranks by low field nuclear resonance. *Energy Geosci.* **2020**, *1*, 93–99. [\[CrossRef\]](#)

23. Lv, Y.M.; Tang, D.Z.; Xu, H.; Luo, H.H. Production characteristics and the key factors in high-rank coalbed methane fields: A case study on the Fanzhuang Block, Southern Qinshui Basin, China. *Int. J. Coal Geol.* **2012**, *96–97*, 93–108. [[CrossRef](#)]
24. Yao, H.F.; Kang, Z.Q.; Li, W. Deformation and reservoir properties of tectonically deformed coals. *Pet. Explor. Dev.* **2014**, *41*, 460–467. [[CrossRef](#)]
25. Gui, B.L. Geological characteristics and enrichment controlling factors of coalbed methane in Liupanshui region. *Acta Petrol. Sin.* **1999**, *20*, 31–37, (In Chinese with English Abstract). [[CrossRef](#)]
26. Li, S.; Tang, D.Z.; Pan, Z.J.; Xu, H.; Guo, L.L. Evaluation of coalbed methane potential of different reservoirs in western Guizhou and eastern Yunnan, China. *Fuel* **2015**, *139*, 257–267. [[CrossRef](#)]
27. Shen, Y.L.; Qin, Y.; Guo, Y.H.; Yi, T.S.; Yuan, X.X.; Shao, Y.B. Characteristics and sedimentary control of a coalbed methane-bearing system in Lopingian (late Permian) coal-bearing strata of western Guizhou Province. *J. Nat. Gas Sci. Eng.* **2016**, *33*, 8–17. [[CrossRef](#)]
28. Luo, W.; Hou, M.C.; Liu, X.C.; Huang, S.G.; Chao, H.; Zhang, R.; Deng, X. Geological and geochemical characteristics of marine-continental transitional shale from the Upper Permian Longtan formation, Northwestern Guizhou, China. *Mar. Pet. Geol.* **2018**, *89 Pt 1*, 58–67. [[CrossRef](#)]
29. Luo, Q.Y.; Xiao, Z.H.; Dong, G.Y.; Ye, X.Z.; Li, H.J.; Zhang, Y.; Ma, Y.; Ma, L.; Xu, Y.H. The geochemical characteristics and gas potential of the Longtan formation in the eastern Sichuan Basin, China. *J. Pet. Sci. Eng.* **2019**, *179*, 1102–1113. [[CrossRef](#)]
30. Shen, S.Z.; Zhang, H.; Zhang, Y.C.; Yuan, D.X.; Chen, B.; He, W.H.; Mu, L.; Lin, W.; Wang, W.Q.; Chen, J.; et al. Permian integrative stratigraphy and timescale of China. *Sci. China Earth Sci.* **2019**, *62*, 154–188. [[CrossRef](#)]
31. Zhang, Y.C.; Li, C.L.; Hong, X.F.; Yuan, Y.C.; Wang, X.H.; Huang, Y.A.; Tang, D.Y.; Zhu, C.S.; Gu, K.S.; Yuan, P.S. *Sedimentary Environments and Coal Accumulation of Late Permian Coal Formation in Southern Sichuan, China*; Guizhou Science and Technology Press: Guiyang, China, 1993; 204p, (In Chinese with English Abstract).
32. China National Administration of Coal Geology. *Sedimentary Environments and Coal Accumulation of Late Permian Coal Formation in Western Guizhou, Southern Sichuan and Eastern Yunnan, China*; Chongqing University Press: Chongqing, China, 1996; 277p, (In Chinese with English Abstract).
33. Dai, S.F.; Zhou, Y.P.; Ren, D.Y.; Wang, X.B.; Li, D.; Zhao, L. Geochemistry and mineralogy of the Late Permian coals from the Songzao Coalfield, Chongqing, southwestern China. *Sci. China-Earth Sci.* **2007**, *50*, 678–688. [[CrossRef](#)]
34. Dai, S.F.; Wang, X.B.; Chen, W.M.; Li, D.H.; Chou, C.L.; Zhou, Y.P.; Zhu, C.S.; Li, H.; Zhu, X.W.; Xing, Y.W.; et al. A high-pyrite semianthracite of Late Permian age in the Songzao Coalfield, southwestern China: Mineralogical and geochemical relations with underlying mafic tuffs. *Int. J. Coal Geol.* **2010**, *83*, 430–445. [[CrossRef](#)]
35. Dai, S.F.; Wang, X.B.; Zhou, Y.P.; Hower, J.C.; Li, D.H.; Chen, W.M.; Zhu, X.W.; Zou, J.H. Chemical and mineralogical compositions of silicic, mafic, and alkali tonsteins in the late Permian coals from the Songzao coalfield, Chongqing, Southwest China. *Chem. Geol.* **2011**, *282*, 29–44. [[CrossRef](#)]
36. Dai, S.F.; Li, T.; Seredin, V.V.; Ward, C.R.; Hower, J.C.; Zhou, Y.P.; Zhang, M.Q.; Song, X.L.; Zhao, C.L. Origin of minerals and elements in the Late Permian coals, tonsteins, and host rocks of the Xinde Mine, Xuanwei, eastern Yunnan, China. *Int. J. Coal Geol.* **2014**, *121*, 53–78. [[CrossRef](#)]
37. Zhao, L.; Ward, C.R.; French, D.; Graham, I.T. Mineralogical composition of Late Permian coal seams in the Songzao Coalfield, southwestern China. *Int. J. Coal Geol.* **2013**, *116–117*, 208–226. [[CrossRef](#)]
38. Tian, X.S.; Shi, Z.J.; Yin, G.; Long, H.Y.; Wang, K. A correlation between the Large Igneous Provinces and mass extinctions: Constraint on the end-Guadalupian mass extinction and the Emeishan LIP in South China, eastern Tethys. *Int. Geol. Rev.* **2016**, *58*, 1215–1233. [[CrossRef](#)]
39. Tian, X.S.; Shi, Z.J.; Yin, G.; Wang, Y.; Tan, Q. Carbonate diagenetic products and processes from various diagenetic environments in Permian paleokarst reservoirs: A case study of the limestone strata of Maokou formation in Sichuan Basin, South China. *Carbonates Evaporites* **2017**, *32*, 215–230. [[CrossRef](#)]
40. Wu, X.J.; Li, Z.F.; Sun, D.F. Coal seam M₈ stoping face water gushing characteristics and countermeasures in Songzao Mining Area. *Coal Geol. China* **2015**, *27*, 35–38, (In Chinese with English Abstract). [[CrossRef](#)]
41. Wu, G.D.; Zeng, C.L.; Cheng, J.; Guo, D.X.; Wang, J.; Wang, D.; Xie, Q.M. Characteristics of groundwater dynamic field and its effect on coalbed methane accumulation in Songzao mining area. *Coal Geol. Explor.* **2018**, *46*, 55–60, (In Chinese with English Abstract). [[CrossRef](#)]
42. SY/T 6414-2014; Maceral Identification and Statistical Methods on Polished Surface of Whole Rocks. Petroleum Geology Exploration Standardization Committee: Beijing, China, 2014. (In Chinese)
43. SY/T 5124-2012; Method of Determining Microscopically the Reflectance of Vitrinite in Sedimentary. Petroleum Geology Exploration Standardization Committee: Beijing, China, 2012. (In Chinese)
44. GB/T 18602-2012; Rock Pyrolysis Analysis. Chinese Standard: Beijing, China, 2012. (In Chinese)
45. SY/T 5162-2014; Analytical Method of Rock Sample by Scanning Electron Microscope. Petroleum Geology Exploration Standardization Committee: Beijing, China, 2014. (In Chinese)
46. Loucks, R.G.; Reed, R.M.; Ruppel, S.C.; Hammes, U. Spectrum of pore types and networks in mudrocks and a descriptive classification for matrix-related mudrock pores. *AAPG Bull.* **2012**, *96*, 1071–1098. [[CrossRef](#)]
47. Kenneth, S.W.S. Characterization of porous solids: An introductory survey. *Stud. Surf. Sci. Catal.* **1991**, *62*, 1–9. [[CrossRef](#)]

48. GB/T 21650.1-2008; Pore Size Distribution and Porosity of Solid Materials by Mercury Porosimetry and Gas Adsorption-Part 1: Mercury Porosimetry. Chinese Standard: Beijing, China, 2008. (In Chinese)
49. SY/T 6385-2016; Porosity and Permeability Measurement under Overburden Pressure. Petroleum Geology Exploration Standardization Committee: Beijing, China, 2016. (In Chinese)
50. GB/T 19559-2008; Method of Determining Coalbed Gas Content. Chinese Standard: Beijing, China, 2008. (In Chinese)
51. Alafnan, S.; Awotunde, A.; Glatz, G.; Adjei, S.; Alrumaih, I.; Gowida, A. Langmuir adsorption isotherm in unconventional resources: Applicability and limitations. *J. Pet. Sci. Eng.* **2021**, *207*, 109172. [[CrossRef](#)]
52. GB/T 13610-2014; Analysis of Natural Gas Composition-Gas Chromatography. Chinese Standard: Beijing, China, 2014. (In Chinese)
53. Dai, S.F.; Bechtel, A.; Eble, C.F.; Flores, R.M.; French, D.; Graham, I.T.; Hood, M.M.; Hower, J.C.; Korasidis, V.A.; Moore, T.A.; et al. Recognition of peat depositional environments in coal: A review. *Int. J. Coal Geol.* **2020**, *219*, 103383. [[CrossRef](#)]
54. Damoulianou, M.E.; Kalaitzidis, S.; Pasadakis, N. Turonian-Senonian organic-rich sedimentary strata and coal facies in Parnassos-Ghiona Unit, Central Greece: An assessment of palaeoenvironmental setting and hydrocarbon generation potential. *Int. J. Coal Geol.* **2022**, *258*, 104029. [[CrossRef](#)]
55. Wang, E.Z.; Guo, T.L.; Liu, B.; Li, M.W.; Xiong, L.; Dong, X.X.; Zhang, N.X.; Wang, T. Lithofacies and pore features of marine-continental transitional shale and gas enrichment conditions of favorable lithofacies: A case study of Permian Longtan Formation in the Lintanchang area, southeast of Sichuan Basin, SW China. *Pet. Explor. Dev.* **2022**, *49*, 1310–1322. [[CrossRef](#)]
56. Abbaszadeh Shahri, A.; Shan, C.L.; Larsson, S. A hybrid ensemble-based automated deep learning approach to generate 3D geo-models and uncertainty analysis. *Eng. Comput.* **2023**. [[CrossRef](#)]
57. Ali, J.R.; Thompson, G.M.; Zhou, M.F.; Song, X.Y. Emeishan large igneous province, SW China. *Lithos* **2005**, *79*, 475–489. [[CrossRef](#)]
58. He, B.; Xu, Y.G.; Wang, Y.M.; Luo, Z.Y. Sedimentation and lithofacies paleogeography in Southwestern China before and after the Emeishan flood volcanism: New Insights into surface response to mantle plume activity. *J. Geol.* **2006**, *114*, 117–132. [[CrossRef](#)]
59. Shellnutt, J.G. The Emeishan large igneous province: A synthesis. *Geosci. Front.* **2014**, *5*, 369–394. [[CrossRef](#)]
60. Xu, Y.G.; Chung, S.L.; Jahn, B.M.; Wu, G.Y. Petrologic and geochemical constraints on the petrogenesis of Permian-Triassic Emeishan flood basalts in southwestern China. *Lithos* **2001**, *58*, 145–168. [[CrossRef](#)]
61. Yang, J.H.; Cawood, P.A.; Du, Y.S.; Huang, H.; Huang, H.W.; Tao, P. Large Igneous Province and magmatic arc sourced Permian-Triassic volcanogenic sediments in China. *Sediment. Geol.* **2012**, *261–262*, 120–131. [[CrossRef](#)]
62. Dai, S.F.; Ward, C.R.; Graham, I.T.; French, D.; Hower, J.C.; Zhao, L.; Wang, X.B. Altered volcanic ashes in coal and coal-bearing sequences: A review of their nature and significance. *Earth-Sci. Rev.* **2017**, *175*, 44–74. [[CrossRef](#)]
63. He, L.J.; Xu, H.H.; Wang, J.Y. Thermal evolution and dynamic mechanism of the Sichuan Basin during the Early Permian-Middle Triassic. *Sci. China-Earth Sci.* **2011**, *54*, 1948–1954. [[CrossRef](#)]
64. Zhu, C.Q.; Hu, S.B.; Qiu, N.S.; Rao, S.; Yuan, Y.S. The thermal history of the Sichuan Basin, SW China: Evidence from the deep boreholes. *Sci. China Earth Sci.* **2016**, *59*, 70–82. [[CrossRef](#)]
65. Zhu, C.Q.; Hu, S.B.; Qiu, N.S.; Jiang, Q.; Rao, S.; Liu, S. Geothermal constraints on Emeishan mantle plume magmatism: Paleotemperature reconstruction of the Sichuan Basin, SW China. *Int. J. Earth Sci.* **2018**, *107*, 71–88. [[CrossRef](#)]
66. Jiang, Q.; Qiu, N.S.; Zhu, C.Q. Heat flow study of the Emeishan large igneous province region: Implications for the geodynamics of the Emeishan mantle plume. *Tectonophysics* **2018**, *724–725*, 11–27. [[CrossRef](#)]
67. He, L.J. Emeishan mantle plume and its potential impact on the Sichuan Basin: Insights from numerical modeling. *Phys. Earth Planet. Inter.* **2022**, *323*, 106841. [[CrossRef](#)]
68. Zhou, Y.P.; Ren, Y.L.; Bohor, B.F. Origin and distribution of tonsteins in late Permian coal seams of Southwestern China. *Int. J. Coal Geol.* **1982**, *2*, 49–77. [[CrossRef](#)]
69. Zhou, Y.P.; Bohor, B.F.; Ren, Y.L. Trace element geochemistry of altered volcanic ash layers (tonsteins) in Late Permian coal-bearing formations of eastern Yunnan and western Guizhou Provinces, China. *Int. J. Coal Geol.* **2000**, *44*, 305–324. [[CrossRef](#)]
70. Shen, M.L.; Dai, S.F.; Rechaev, V.P.; French, D.; Graham, I.T.; Liu, S.D.; Chekryzhov, I.Y.; Tarasenko, I.A.; Zhao, S.W. Provenance changes for mineral matter in the latest Permian coals from western Guizhou, southwestern China, relative to tectonic and volcanic activity in the Emeishan Large Igneous Province and Paleo-Tethys region. *Gondwana Res.* **2023**, *113*, 71–88. [[CrossRef](#)]
71. Chen, Z.S.; Wu, Y.D. Late Permian Emeishan basalt and coal-bearing formation in southern Sichuan area. *Coal Geol. China* **2010**, *22*, 14–18, (In Chinese with English Abstract). [[CrossRef](#)]
72. Feng, Q.Q.; Qiu, N.S.; Fu, X.D.; Li, W.Z.; Xu, Q.; Li, X.; Wang, J.S. Permian geothermal units in the Sichuan Basin: Implications for the thermal effect of the Emeishan mantle plume. *Mar. Pet. Geol.* **2021**, *132*, 105226. [[CrossRef](#)]
73. He, B.; Xu, Y.G.; Chung, S.L.; Xiao, L.; Wang, Y.M. Sedimentary evidence for a rapid, kilometer-scale crustal doming prior to the eruption of the Emeishan flood basalts. *Earth Planet. Sci. Lett.* **2003**, *213*, 391–405. [[CrossRef](#)]
74. Tang, S.L.; Tang, D.Z.; Li, S.; Xu, H.; Tao, S.; Geng, Y.G.; Ma, L.; Zhu, X.G. Fracture system identification of coal reservoir and the productivity differences of CBM wells with different coal structures: A case in the Yanchuannan Block, Ordos Basin. *J. Pet. Sci. Eng.* **2018**, *161*, 175–189. [[CrossRef](#)]
75. Ju, Y.W.; Qiao, F.; Wei, M.M.; Li, X.; Xu, F.Y.; Feng, G.R.; Li, Y.; Wu, C.F.; Cao, Y.X.; Li, G.F.; et al. Typical coalbed methane (CBM) enrichment and production modes under the control of regional structure and evolution. *Coal Geol. Explor.* **2022**, *50*, 2, (In Chinese with English Abstract). [[CrossRef](#)]

76. Song, Y.; Liu, H.L.; Feng, H.; Qin, S.F.; Liu, S.B.; Li, G.Z.; Zhao, M.J. Syncline reservoir pooling as a general model for coalbed methane (CBM) accumulations: Mechanisms and case studies. *J. Nat. Gas Sci. Eng.* **2012**, *88–89*, 5–12. [[CrossRef](#)]
77. Chen, Y.; Tang, D.Z.; Xu, H.; Li, Y.; Meng, Y.J. Structural controls on coalbed methane accumulation and high production models in the eastern margin of Ordos Basin, China. *J. Nat. Gas Sci. Eng.* **2015**, *23*, 524–537. [[CrossRef](#)]

Disclaimer/Publisher’s Note: The statements, opinions and data contained in all publications are solely those of the individual author(s) and contributor(s) and not of MDPI and/or the editor(s). MDPI and/or the editor(s) disclaim responsibility for any injury to people or property resulting from any ideas, methods, instructions or products referred to in the content.